Quantum theory of photon emission during strong-laser-field-induced ionization

D. B. Milošević
University of Sarajevo, Faculty of Science, 71000 Sarajevo, Bosnia and Herzegovina
and Academy of Sciences and Arts of Bosnia and Herzegovina, 71000 Sarajevo, Bosnia and Herzegovina

(Received 10 June 2023; accepted 12 September 2023; published 22 September 2023)

We formulate a quantum theory of photon emission during strong-laser-field-induced ionization and show that such photons can be emitted in a single-step process. The probability of this process is many orders of magnitude higher than that of the well-known high-order harmonic generation, which is a three-step process. We analyzed photon emission for various wavelengths and intensities of the laser field and found that the probability of photon emission is maximal for energies near 5 eV and that it can be shifted to higher energies for higher intensity. For a bichromatic linearly polarized laser field the photon emission rate can be controlled with the relative phase between the field components and can be one order of magnitude higher than in the monochromatic case. For circular laser polarization the rate of photon emission is lower than for the linear one and it depends on the emitted photon direction (it is much lower if the emitted photon polarization is perpendicular to the laser-field polarization plane). For the counterrotating bicircular field the rate is much higher than for the corotating bicircular field, monochromatic circularly and linearly polarized fields, and bichromatic linearly polarized field. The rate is the highest for orthogonally polarized two-color field for the relative phase $\pi/2$.

DOI: 10.1103/PhysRevA.108.033110

I. INTRODUCTION

Over the past few decades the advances in photonic physics are based on new light sources, from ultrastrong laser pulses [1] and attosecond light sources [2] to synchrotron radiation and x-ray free electron lasers [3]. At ELI-Beamlines [4] ultrahigh laser intensities ($>10^{22}$ W/cm^2) are in reach [5,6]. Particularly interesting is high-order harmonic generation (HHG), discovered more than a quarter of a century ago [7,8], since it opened up the era of attoscience [2]. HHG is a three-step process induced by a strong laser pulse. In the first step, an electron is temporarily liberated from the atom and, in the second step, it is driven by the laser field away from and back to the parent ion. In the third step, this electron recombines with the parent ion and a harmonic photon is emitted. The energy of the harmonic photon is equal to the sum of the ionization potential and the energy accumulated by the laser-driven electron. In addition, HHG radiation is coherent and ultrashort. The HHG process is closely related to another laser-field-induced process, above-threshold ionization (ATI), in which more photons are absorbed from the laser field than is necessary for ionization, thus allowing emission of high-energy electrons [9]. In most theoretical treatment of HHG and ATI the laser field is considered a classical electromagnetic field. More recently, a fully quantized approach is developed [10–15] that allows us to consider the dynamics of these processes from a novel perspective by taking into account the quantum nature of electromagnetic field. For example, light-matter entanglement after ATI was considered in Ref. [11].

In the present contribution, we will show that during ATI the high-energy photons can also be emitted in a one-step process. This process is schematically presented in Fig. 1 (right panel: ATI-PhE process), together with the above-mentioned ATI and HHG processes. For analysis of this process we will formulate a theory in which the laser field is treated classically, while the emitted photon field is quantized. This approach is similar to that developed earlier for treatment of x-ray–atom scattering in the presence of a laser field [16] and HHG [17,18] (see also the review article [19]). The general framework laid out by Rivera-Dean *et al.* [11] would allow one to calculate ATI contingent with emission of an arbitrary non-laser photon, but no explicit expressions have been presented. Here our focus is the calculation of emission rates of such photons, rather than expressions for the electron-field entanglement. We apply our theory to calculate the corresponding

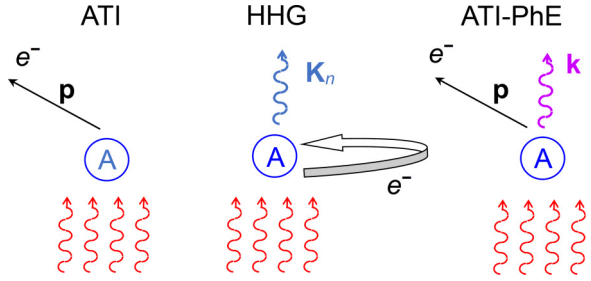

FIG. 1. Schematic presentation of the strong-laser-field-induced processes: above-threshold ionization (left panel), high-order harmonic generation (middle panel), and photon emission during above-threshold ionization (ATI-PhE; right panel). Induced by a strong laser field (red curved lines), atom (A) is ionized and an electron (e^-; black solid line) with the momentum **p** is emitted. In the HHG process an nth harmonic photon with the wave vector $\mathbf{K}_n$ is emitted, and the temporarily liberated electron returns and recombines with the parent ion. In the ATI-PhE process both the electron with the momentum **p** and a photon with the wave vector **k** (pink curved line) are emitted.

emitted photon spectra. Since the ATI electrons can be emitted in arbitrary directions, in order to obtain the rate of photon emission, we have to integrate over all final electron momenta, which makes numerical calculations more time-consuming.

In Sec. II, using the S-matrix formalism and the strong-field approximation (SFA), we derive an expression for the rate of photon emission during ATI. We apply this theory to obtain numerical results for the photon emission rate, first for a linearly polarized laser field in Sec. III A and then for a bichromatic elliptically polarized laser field in Sec. III B. Our conclusions and discussions are given in Sec. IV. Atomic units are used ($e = \hbar = m_e = 4\pi\varepsilon_0 = 1$).

II. THEORY

S-matrix formalism is usually used in scattering theory [20,21]. It can also be applied to strong-field physics. It is particularly useful for ATI (see, for example, Ref. [9] and references therein; important was the application of the S-matrix theory to the development of the SFA, which is often called Keldysh-Faisal-Reiss theory [22–24]). This formalism was also successfully applied to HHG [17–19]. More recently, in Ref. [25], which addressed the SFA and quantum orbits, we applied the S-matrix theory to ATI and HHG in a unified way. In the present work, we apply this theory to a situation where a photon is emitted (like in HHG), but the final state, instead of a bound state (as in HHG), is a continuum state, i.e., a photoelectron is emitted (like in ATI). We will follow the formalism of Ref. [25]. The general S-matrix element for transition from an initial state i (in state) to a final state f (out state) is

$$S_{fi} = i \lim_{t\to\infty} \lim_{t'\to-\infty} \langle \Phi_{\rm out}(t)|G^{(+)}_{\rm tot}(t,t')|\Phi_{\rm in}(t')\rangle, \quad (1)$$

where the total Green's operator $G^{(+)}_{\rm tot}(t,t')$ corresponds to the Hamiltonian

$$H_{\rm tot}(t) = H(t) + V_{\rm ph}(t), \;\; H(t) = H_0 + V_{\rm le}(t) + V_{\rm at}(\mathbf{r}). \quad (2)$$

Here $V_{\rm ph}(t) = \mathbf{r}\cdot\mathbf{E}_{\rm ph}(t)$ is the interaction (in length gauge and dipole approximation) of our system (atom or molecule or the corresponding ions; for simplicity, we will refer to our system as an atom) with the quantized photon field [26],

$$\mathbf{E}_{\rm ph}(t) = \sum_{\mathbf{k}} c_k \left(a^\dagger_{\mathbf{k}} e^{i\omega_k t}\hat{\mathbf{e}}^*_{\mathbf{k}} - a_{\mathbf{k}} e^{-i\omega_k t}\hat{\mathbf{e}}_{\mathbf{k}}\right), \quad (3)$$

where $c_k = -i(2\pi\omega_k/V)^{1/2}$, with V the quantization volume, and $a_{\mathbf{k}}$ and $a^\dagger_{\mathbf{k}}$ the annihilation and creation operators of the emitted photon having the frequency $\omega_k = k^2/2$ ($k = |\mathbf{k}|$), wave vector $\mathbf{k}$, and complex unit polarization vector $\hat{\mathbf{e}}_{\mathbf{k}}$. In the second equation in (2) it is $H_0 = -\nabla^2/2$ with $\nabla \equiv \partial/\partial\mathbf{r}$, $V_{\rm le}(t) = \mathbf{r}\cdot\mathbf{E}(t)$ is the interaction of the laser field [described by the electric field vector $\mathbf{E}(t)$] with the electron, and $V_{\rm at}(\mathbf{r})$ is the atomic interaction. Strong laser field, with a large number of photons in a mode, is treated classically, while the weak emitted photon field, having one or zero photons in a mode, is quantized. We further suppose that the in and out states are

$$|\Phi_{\rm in}(t)\rangle = |\psi_b\rangle e^{iI_p t}|0_{\mathbf{k}}\rangle, \quad |\Phi_{\rm out}(t)\rangle = |\psi_{\mathbf{p}}\rangle e^{-iE_p t}|1_{\mathbf{k}}\rangle, \quad (4)$$

where $|\psi_b\rangle$ and $|\psi_{\mathbf{p}}\rangle$ are the solutions of the laser- and photon-free stationary Schrödinger equation with the Hamiltonian $H_{\rm at} = H_0 + V_{\rm at}(\mathbf{r})$, I_p is the ionization potential of the atomic bound state, and $E_p = p^2/2$ is the emitted photoelectron kinetic energy ($p \equiv |\mathbf{p}|$, with $\mathbf{p}$ the electron momentum). The interaction with the laser field is off for the in and out states. There is no photons in the in state and the corresponding ket vector is $|0_{\mathbf{k}}\rangle$, while one new photon with the wave vector $\mathbf{k}$ and the ket vector $|1_{\mathbf{k}}\rangle$ is generated in the out state. The total Green's operator satisfies the Lippmann-Schwinger equation,

$$G^{(+)}_{\rm tot}(t,t') = G^{(+)}(t,t') + \int d\tau G^{(+)}_{\rm tot}(t,\tau)V_{\rm ph}(\tau)G^{(+)}(\tau,t'). \quad (5)$$

Inserting this into Eq. (1), using Eqs. (2) and (3), and the relations $a_{\mathbf{k}}|0_{\mathbf{k}}\rangle = 0$, $a^\dagger_{\mathbf{k}}|0_{\mathbf{k}}\rangle = |1_{\mathbf{k}}\rangle$, and $\langle 1_{\mathbf{k}}|G^{(+)}_{\rm tot}(t,\tau)|1_{\mathbf{k}}\rangle = G^{(+)}(t,\tau)$, we get

$$S_{fi} = -ic_k \int_{-\infty}^{\infty} dt e^{i\omega_k t}\hat{\mathbf{e}}^*_{\mathbf{k}}\cdot\mathbf{d}_{fi}(t), \quad (6)$$

where $\mathbf{d}_{fi}(t)$ is the time-dependent dipole matrix element between the initial and final laser-dressed states,

$$\mathbf{d}_{fi}(t) = \langle \Phi^{(-)}_f(t)|\mathbf{r}|\Phi^{(+)}_i(t)\rangle, \quad (7)$$

with

$$\langle \Phi^{(-)}_f(\tau)| = i\lim_{t'\to\infty} e^{iE_{p}t'}\langle\psi_{\mathbf{p}}|G^{(+)}(t',\tau),$$
$$|\Phi^{(+)}_i\tau)\rangle = i\lim_{t\to-\infty} G^{(+)}(\tau,t)|\psi_b\rangle e^{iI_p t}. \quad (8)$$

In the SFA we approximate the state $|\Phi^{(-)}_f(\tau)\rangle$ with the Volkov state,

$$|\chi_{\mathbf{p}}(\tau)\rangle = |\mathbf{p}+\mathbf{A}(\tau)\rangle e^{-iS_{\mathbf{p}}(\tau)}, \;\; dS_{\mathbf{p}}(\tau)/d\tau = [\mathbf{p}+\mathbf{A}(\tau)]^2/2, \quad (9)$$

which is a solution of the time-dependent Schrödinger equation with the Hamiltonian $H_0 + V_{\rm le}(\tau)$, $|\mathbf{p}+\mathbf{A}(\tau)\rangle$ is a ket vector such that $\langle\mathbf{r}|\mathbf{p}+\mathbf{A}(\tau)\rangle = e^{i[\mathbf{p}+\mathbf{A}(\tau)]\cdot\mathbf{r}}/(2\pi)^{3/2}$ is a plane wave, and $\mathbf{A}(\tau) = -\int^\tau dt\mathbf{E}(t)$. The state $|\Phi^{(+)}_i(\tau)\rangle$ satisfies the Lippmann-Schwinger equation,

$$|\Phi^{(+)}_i(\tau)\rangle = |\psi_b(\tau)\rangle + \int dt G^{(+)}(\tau,t)V_{\rm at}(t)|\psi_b(t)\rangle, \quad (10)$$

and, in the lowest order, it can be approximated by the atomic bound state, so that our final result for the S-matrix element in the SFA is

$$S_{\mathbf{p}}(\omega_k,\hat{\mathbf{e}}_{\mathbf{k}}) = -ic_k\int_{-\infty}^{\infty} dt e^{i\omega_k t}\langle\chi_{\mathbf{p}}(t)|\hat{\mathbf{e}}^*_{\mathbf{k}}\cdot\mathbf{r}|\psi_b(t)\rangle. \quad (11)$$

We suppose that the fundamental frequency of the laser field is $\omega = 2\pi/T$, with T the period of the laser field, and introduce the notation $\boldsymbol{\alpha}(t) = \int^t dt'\mathbf{A}(t')$, $U_1(t) = \int^t dt'\mathbf{A}^2(t')/2 - U_p t$, with $U_p = \int_0^T dt\mathbf{A}^2(t)/2$ the ponderomotive energy, so that $S_{\mathbf{p}}(t) = E_p t + \mathbf{p}\cdot\boldsymbol{\alpha}(t) + U_1(t) + U_p t$. For a T-periodic laser field, we can expand the T-periodic part of the subintegral function in Eq. (11),

$$\mathcal{T}_{\mathbf{p}}(t) = \langle\mathbf{p}+\mathbf{A}(t)|\mathbf{r}|\psi_b\rangle e^{i[\mathbf{p}\cdot\boldsymbol{\alpha}(t)+U_1(t)]}, \quad (12)$$

into a Fourier series as

$$\mathcal{T}_{\mathbf{p}}(t) = \sum_{n=-\infty}^{\infty} \mathbf{T}_{\mathbf{p}}(n) e^{-in\omega t}, \ \mathbf{T}_{\mathbf{p}}(n) = \int_0^T \frac{dt}{T} \mathcal{T}_{\mathbf{p}}(t) e^{in\omega t}. \tag{13}$$

Denoting $E = \omega_k + I_p + U_p + E_p$, we can rewrite the integral $\int_{-\infty}^{\infty} dt \cdots$ in Eq. (11) as $\sum_{n=-\infty}^{\infty} \int_{nT}^{(n+1)T} dt\, \hat{\mathbf{e}}_{\mathbf{k}}^* \cdot \mathcal{T}_{\mathbf{p}}(t) e^{iEt} = \int_0^T dt' \hat{\mathbf{e}}_{\mathbf{k}}^* \cdot \mathcal{T}_{\mathbf{p}}(t') \sum_{n=-\infty}^{\infty} e^{iE(t'+nT)}$, where we made the substitution $t' = t - nT$ and used the T-periodicity of the function $\mathcal{T}_{\mathbf{p}}(t')$, $\mathcal{T}_{\mathbf{p}}(t'+nT) = \mathcal{T}_{\mathbf{p}}(t')$. Using the relation $\sum_n e^{iEnT} = \omega \sum_n \delta(E - n\omega)$ and Eq. (13), we finally get

$$S_{\mathbf{p}}(\omega_k, \hat{\mathbf{e}}_{\mathbf{k}}) = -2\pi i c_k \sum_n \delta(E - n\omega) \hat{\mathbf{e}}_{\mathbf{k}}^* \cdot \mathbf{T}_{\mathbf{p}}(n). \tag{14}$$

Further, we have $|S_{\mathbf{p}}(\omega_k, \hat{\mathbf{e}}_{\mathbf{k}})|^2 = 4\pi^2 |c_k|^2 \sum_n \delta(E - n\omega) \hat{\mathbf{e}}_{\mathbf{k}}^* \cdot \mathbf{T}_{\mathbf{p}}(n) \sum_{n'} \delta(E - n'\omega) \hat{\mathbf{e}}_{\mathbf{k}} \cdot \mathbf{T}_{\mathbf{p}}^*(n')$, so that, using the relations $|c_k|^2 = 2\pi\omega_k/V$ and $\delta(E - n'\omega) = \lim_{\tau_p \to \infty} \int_{-\tau_p/2}^{\tau_p/2} dt e^{i(E-n'\omega)t}$, which is equal to $\tau_p/(2\pi)$ for $n'\omega = E$ and vanishes elsewhere (τ_p is the laser pulse duration), we get

$$\frac{|S_{\mathbf{p}}(\omega_k, \hat{\mathbf{e}}_{\mathbf{k}})|^2}{\tau_p} = 4\pi^2 \frac{2\pi\omega_k}{V} \frac{1}{2\pi} \sum_n \delta(E - n\omega) |\hat{\mathbf{e}}_{\mathbf{k}}^* \cdot \mathbf{T}_{\mathbf{p}}(n)|^2. \tag{15}$$

We want to obtain the rate (probability per unit time)

$$w_{\mathbf{p}}(\omega_k, \hat{\mathbf{e}}_{\mathbf{k}}) = \frac{d}{d\Omega_{\hat{\mathbf{k}}}} \sum_{\mathbf{k}'}{}' |S_{\mathbf{p}}(\omega_{k'}, \hat{\mathbf{e}}_{\mathbf{k}'})|^2 / \tau_p \tag{16}$$

of emission of a photon, having the frequency within the interval $(\omega_k - \epsilon, \omega_k + \epsilon)$ and the polarization $\hat{\mathbf{e}}_{\mathbf{k}}$, into a solid angle $d\Omega_{\hat{\mathbf{k}}}$, with simultaneous emission of an electron with the momentum $\mathbf{p}$. For this purpose we use the connection $\sum_{\mathbf{k}'}{}' \to V \int' d^3\mathbf{k}'/(2\pi)^3 = V \int_{\omega_k - \epsilon}^{\omega_k + \epsilon} d\omega_{k'} \omega_{k'}^2 \int d\Omega_{\hat{\mathbf{k}}'}/(2\pi c)^3$, where the prime over the sum and over the integral denotes that we selected an interval around the frequency $\omega_k = kc$ such that ϵ is small enough so that $\omega_{k'}^2 |S_{\mathbf{p}}(\omega_{k'}, \hat{\mathbf{e}}_{\mathbf{k}'})|^2$ is almost constant in the interval of integration. The delta function in (15) cancels both the integral over $d\omega_{k'}$ and the sum over n, retaining only the energy-conservation term, so that the final result is (for a similar derivation for the case of x-ray–atom scattering in the presence of a laser field see Ref. [16])

$$w_{\mathbf{p}}(\omega_k, \hat{\mathbf{e}}_{\mathbf{k}}) = \frac{\omega_k^3}{2\pi c^3} \left| \hat{\mathbf{e}}_{\mathbf{k}}^* \cdot \mathbf{T}_{\mathbf{p}}(n) \right|^2_{/n=(\omega_k + I_p + U_p + E_p)/\omega}. \tag{17}$$

Here $\mathbf{T}_{\mathbf{p}}(n)$ is the T-matrix vector for emission of a photon with the frequency ω_k during ionization from the initial bound state to the final continuum state with the electron momentum $\mathbf{p}$. In this process n photons are absorbed from the laser field and the energy-conservation condition is

$$\omega_k = n\omega - I_p - U_p - E_p. \tag{18}$$

Since we are interested only in the photon emission, we integrate over the electron momenta and get the (total) rate,

$$W(\omega_k, \hat{\mathbf{e}}_{\mathbf{k}}) = \int d^3\mathbf{p}\, w_{\mathbf{p}}(\omega_k, \hat{\mathbf{e}}_{\mathbf{k}}). \tag{19}$$

III. NUMERICAL RESULTS

A. Linear polarization

We first illustrate the above results using a linearly polarized bichromatic laser field $\mathbf{E}(t) = E(t)\hat{\mathbf{e}}$ [27],

$$E(t) = E_1 \sin\omega t + E_2 \sin(2\omega t + \phi), \tag{20}$$

with the components amplitudes E_1 and E_2 and the relative phase ϕ. For this field we have $A(t) = A_1 \cos\omega t + A_2 \cos(2\omega t + \phi)$, $\alpha(t) = \alpha_1 \sin\omega t + \alpha_2 \sin(2\omega t + \phi)$, $U_p = U_{p1} + U_{p2}$, $U_{pj} = A_j^2/4$, $A_j = E_j/(j\omega)$, $\alpha_j = A_j/(j\omega)$, $j = 1, 2$, and $4\omega U_1(t) = 2U_{p1} \sin(2\omega t) + U_{p2} \sin(4\omega t + 2\phi) + 8\sqrt{U_{p1}U_{p2}}[\sin(\omega t + \phi) + \sin(3\omega t + \phi)/3]$. We use the hydrogen-like atom model from Ref. [28] [see Eq. (45) therein].

In the spherical coordinates the integral over the electron momenta $\int d^3\mathbf{p}$ in Eq. (19) can be transformed as

$$\int_0^\infty dp\, p^2 \int_0^\pi d\theta_p \sin\theta_p \int_0^{2\pi} d\varphi_p \to 2\pi \int_0^\infty dE_p\, p \int_{-1}^1 dx$$

$$\to 2\pi \sum_{n>n_0} p \int_{-1}^1 dx, \ n_0 = [(\omega_k + I_p + U_p)/\omega], \tag{21}$$

where we supposed that the subintegral function does not depend on the angle φ_p, made the substitution $x = \cos\theta_p$, and used the condition (18) to replace the integral $\int dE_p$ with the sum over the number of absorbed photons n. In this case Eq. (19) reduces to

$$W(\omega_k, \hat{\mathbf{e}}_{\mathbf{k}}) = \frac{\omega_k^3}{2\pi c^3} \frac{2^7}{\pi} (2I_p)^{5/2} 2\pi \sum_{n>n_0} p \int_{-1}^1 dx |f_n(x)|^2, \tag{22}$$

with $p = \sqrt{2(n\omega - \omega_k - I_p - U_p)}$, $\hat{\mathbf{e}}_{\mathbf{k}} = \hat{\mathbf{e}}$, and

$$f_n(x) = \int_0^T \frac{dt}{T} \frac{[px + A(t)] e^{i[U_1(t) + p\alpha(t)x + n\omega t]}}{[p^2 + A^2(t) + 2pA(t)x + 2I_p]^3}. \tag{23}$$

Before we present the results for the total rate, Eq. (22), it is illustrative to present the rate for simultaneous emission of a photon and an electron with the energy E_p:

$$W_{E_p}(\omega_k, \hat{\mathbf{e}}_{\mathbf{k}}) = \int d\Omega_{\hat{\mathbf{p}}}\, w_{\mathbf{p}}(\omega_k, \hat{\mathbf{e}}_{\mathbf{k}}). \tag{24}$$

This rate is presented in Fig. 2 in the ω_k-E_p plane for ATI of argon atoms ($I_p = 15.76$ eV) by a linearly polarized monochromatic laser field $E(t) = E_1 \cos\omega t$, $E_2 = 0$, $U_p = U_{p1}$, with the intensity 2×10^{14} W/cm^2 and the fundamental wavelength 1800 nm (upper panel) and 1200 nm (lower panel). Since $E_p = n\omega - \omega_k - I_p - U_p > 0$ the minimum number of absorbed photons is $n_{\min}(\omega_k) = [(\omega_k + I_p + U_p)/\omega] + 1$. We see that the rate is maximum for low photoelectron energies and decreases with an increase of the photoelectron energy. Also, the rate is maximum for emitted photon energies ω_k below $0.1U_p$ for laser-field wavelength 1800 nm. This maximum is shifted to $0.2U_p$ for 1200 nm. For higher and lower photon energies the rate decreases exponentially.

According to the results presented in Fig. 2, we expect that the total rate $W(\omega_k, \hat{\mathbf{e}})$ as a function of ω_k exhibits a

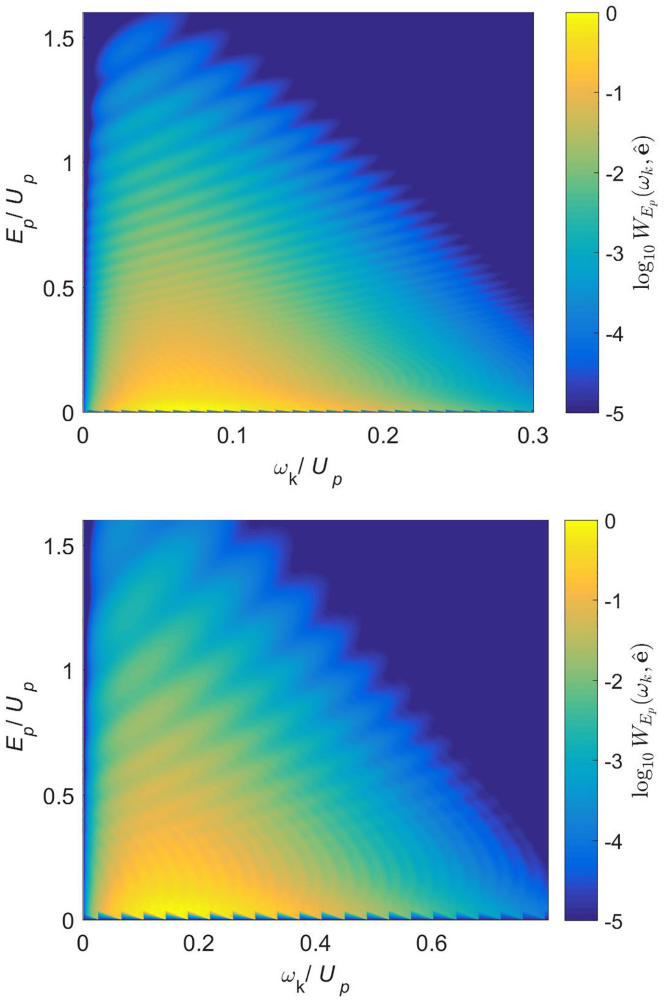

FIG. 2. Logarithm of the rate $W_{E_p}(\omega_k, \hat{\mathbf{e}})$, Eq. (24), presented in the emitted photon energy ω_k-photoelectron kinetic energy E_p plane (in units of the ponderomotive energy U_p) for ATI of argon atoms by a linearly polarized monochromatic laser field with the intensity 2×10^{14} W/cm^2 and the wavelengths 1800 nm (upper panel) and 1200 nm (lower panel). The rate is normalized to unity and the false-color scale covers five orders of magnitude.

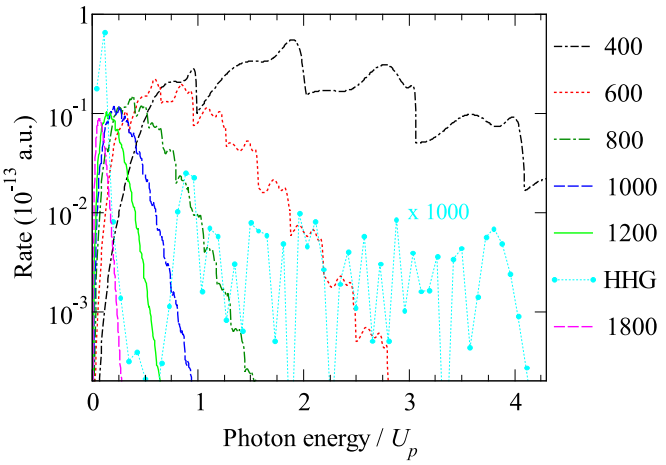

FIG. 3. The total rate $W(\omega_k, \hat{\mathbf{e}})$, Eq. (22), as a function of the emitted photon energy ω_k in units of the ponderomotive energy U_p for photon emission during ATI of argon atoms by a linearly polarized monochromatic laser field with the intensity 2×10^{14} W/cm^2 and wavelength in nanometers, as denoted in the legend. The HHG rate, for the wavelength 1200 nm and other parameters the same, is shown by a cyan line with circles and is multiplied by the factor 1000.

maximum and that this maximum shifts to the higher values (in units of U_p) with a decrease of the laser wavelength. In order to check this, in Figs. 3–6 we show the results for the total rate obtained by numerical integration for different laser wavelengths and intensities but for the same other laser and atomic parameters as in Fig. 2. First, in Fig. 3 we show the results for the intensity 2×10^{14} W/cm^2, the fundamental wavelength from 400 to 1200 nm, in steps of 200 nm, and for the fundamental wavelength 1800 nm. The total rate is the highest for the shortest wavelength and exhibits an oscillatory structure. With the increase of the wavelength this rate decreases and an isolated maximum appears. With a further increase of the wavelength, this maximum is becoming narrower, having fewer oscillations, and shifts to lower photon energies. For 600, 800, 1000, and 1200 nm its position is below $1U_p$, $0.4U_p$, $0.25U_p$, and $0.15U_p$, respectively. For comparison we have presented the HHG rate, calculated using SFA [18,19,25,29,30], by argon atoms for the intensity 2×10^{14} W/cm^2 and wavelength 1200 nm. The discrete odd harmonics form a plateau, having the length $I_p + 3.17U_p$. This HHG plateau is more than four orders of magnitude lower than our photon emission rate $W(\omega_k, \hat{\mathbf{e}})$. Therefore, photon emission during ATI is much more efficient than HHG, the spectrum is continuous, and the emitted photon energies are lower.

Let us now further explore how the total photon emission rate changes with the increase of the laser wavelength and intensity. From the upper panel of Fig. 4 we see that the rate slightly decreases with the increase of the wavelength. As in Fig. 3, the spectrum forms a peak which becomes narrower and shifts to lower energies (in units of U_p) with the increase of the wavelength. If we present the spectrum in units of electronvolts (see the lower panel of Fig. 4), then all curves are in the region from 2.5 to 10 eV (full width at half maximum is 7.5 eV) with a maximum near 5.5 eV. From Fig. 5 we see that, with the increase of the laser intensity, the rate can increase by orders of magnitude, while the peak position is shifted to slightly lower energies. For the used wavelength of 1030 nm, the ponderomotive energy is $U_p = 19.81$ eV for the intensity 2×10^{14} W/cm^2 ($j = 2$ in Fig. 5) and 118.9 eV for the six-times-higher intensity ($j = 12$).

For higher laser intensities we should take into account that argon atoms can be completely ionized. In Table I we present the critical intensity according the barrier-suppression ionization model [31]. For the intensity below 2.47×10^{14} W/cm^2 the ionization potential of the Ar atom should be used, while for the intensity interval $\{2.47, 5.83\} \times 10^{14}$ W/cm^2 the calculations should be done for the ionization potential $I_p = 27.63$ eV of the ion Ar^+, etc. In Fig. 6, for the fixed laser wavelength of 800 nm, we present the results for the intensities $\{2, 5, 12, 30, 50, 77, 195, 260\} \times 10^{14}$ W/cm^2,

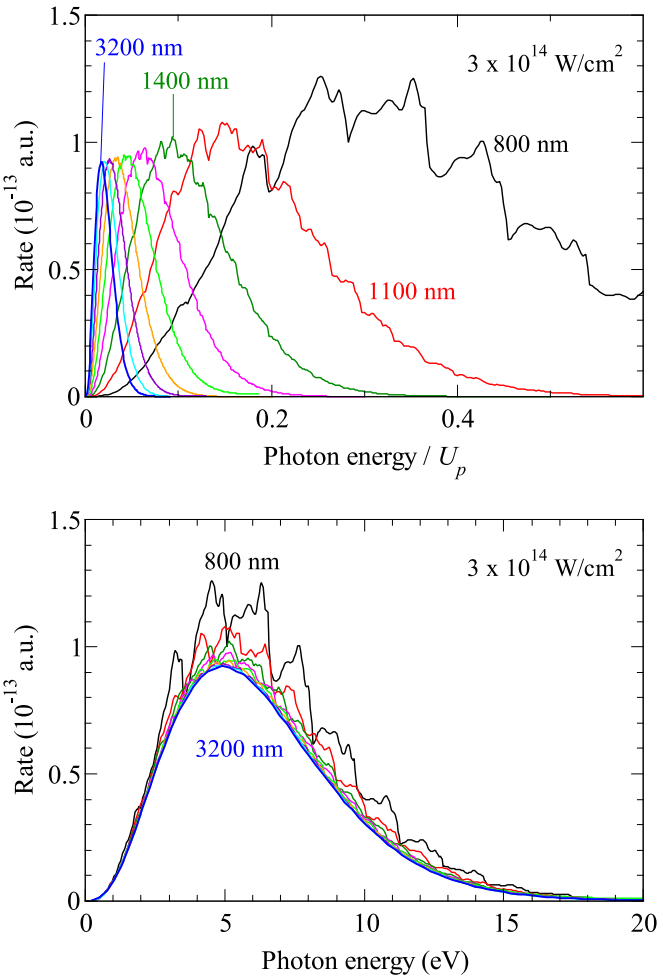

FIG. 4. The total rate $W(\omega_k, \hat{\mathbf{e}})$ as a function of the emitted photon energy ω_k in units of U_p (upper panel) and in units of eV (lower panel), presented similarly as in Fig. 3 but on a linear scale and for the fixed laser intensity 3×10^{14} W/cm^2. The wavelength changes from 800 to 3200 nm, in steps of 300 nm.

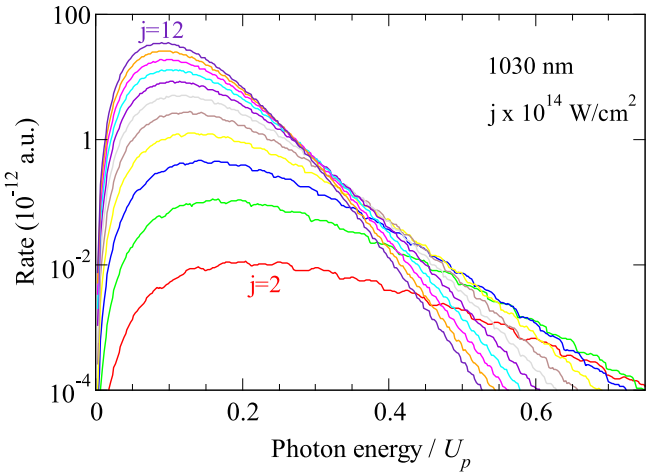

FIG. 5. The total rate $W(\omega_k, \hat{\mathbf{e}})$, presented similarly as in Fig. 3 but for the fixed laser wavelength of 1030 nm. The laser intensity is $j \times 10^{14}$ W/cm^2, where $j = 2, 3, \ldots, 12$, from the bottom to the top curve.

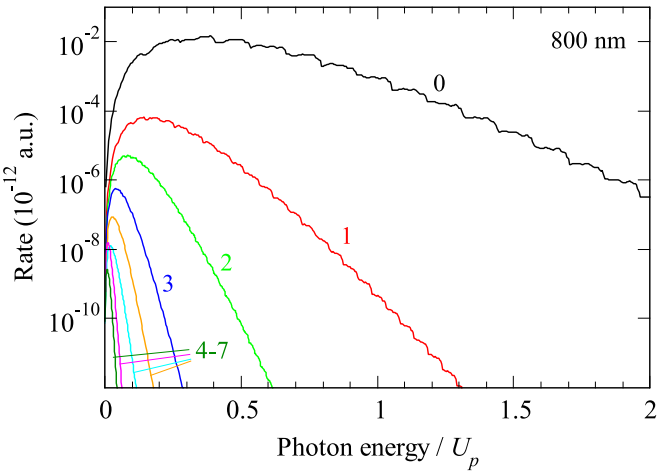

FIG. 6. The total rate $W(\omega_k, \hat{\mathbf{e}})$, presented similarly as in Fig. 3 but for a fixed wavelength of 800 nm, and different Ar^{Z+} ions, with the values of Z denoted in the figure. The corresponding intensities are given in the text.

which correspond to the charges $Z = \{0, 1, 2, 3, 4, 5, 6, 7\}$ of the Ar^{Z+} ion, as denoted in the figure. We see that the total rates decrease with the increase of Z and that the spectra become narrower (as a function of U_p) with the maximum shifted to lower energies. In electronvolts the maximum shifts from 5 eV for $Z = 0$ to 14 eV for $Z = 7$.

Let us now present the results for a linearly polarized bichromatic laser field. We use argon atoms and a laser field with the fundamental wavelength 1030 nm and the components intensities $I_1 = E_1^2 = I_2 = E_2^2 = 1.5 \times 10^{14}$ W/cm^2. In Fig. 7 we show how the rate $W(\omega_k, \hat{\mathbf{e}})$ depends on the emitted photon energy. The total rate exhibits the maximum for the energy near $0.5U_{p1} = 7.43$ eV for all relative phases. It is maximal for the phase $\phi = \pi/2$. We also presented the result for a monochromatic laser field with $I_{2\omega} = 0$ and two times higher intensity of the first component (3×10^{14} W/cm^2; for comparison with other results shown in Fig. 7, this result is presented by a magenta double-dot-dashed line and in units of the ponderomotive energy which corresponds to the intensity 1.5×10^{14} W/cm^2). We see that the rate for the monohromatic field is lower by an order of magnitude and that the maximum is shifted to the lower photon energy. Similarly as in Fig. 2, in Fig. 8 the present the rate $W_{E_p}(\omega_k, \hat{\mathbf{e}})$ for the phase $\phi = \pi/2$ (other parameters are the same as in Fig. 7). We see that the maximum photon energy is shifted to higher values than in the monochromatic case and that higher photoelectron energies contribute (compare with Fig. 2).

TABLE I. Ionization potential of Ar^{Z+} ions and the critical intensity $I_{\rm BSI}$ (10^9 W/cm^2) $= [2I_p^2$ (eV)$/(Z+1)]^2$ according to the barrier-suppression ionization model [31].

Z	0	1	2	3	4	5	6	7
I_p (eV)	15.8	27.6	40.7	59.6	74.8	91.3	124	144
$I_{\rm BSI}$ (10^{14} W/cm^2)	2.47	5.83	12.2	31.5	50.2	77.2	196	265

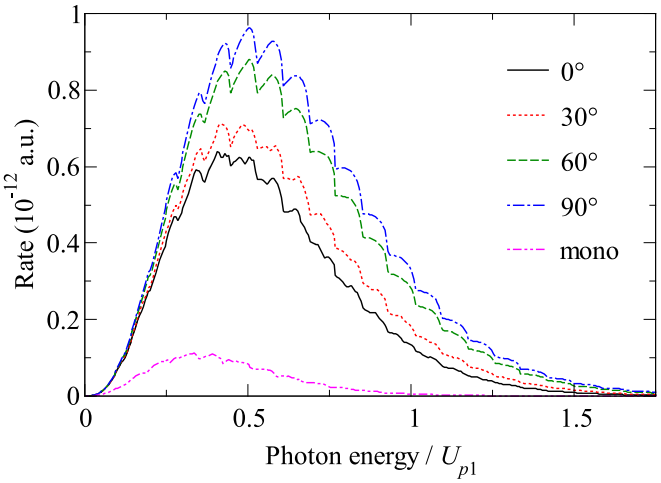

FIG. 7. The total rate $W(\omega_k, \hat{\mathbf{e}})$, Eq. (22), as a function of the emitted photon energy in units of the ponderomotive energy U_{p1} for photon emission during ATI of argon atoms by a linearly polarized bichromatic laser field (20) with equal components intensities $I_1 = I_2 = 1.5 \times 10^{14}$ W/cm^2, the fundamental wavelength 1030 nm, and the relative phase ϕ, as denoted in the legend. The result for the monochromatic field having the intensity $2I_1$ is presented by a magenta double-dot-dashed line.

B. Elliptical polarization

As the next example, we present numerical results for an elliptically polarized monochromatic laser field defined in the xy plane:

$$\mathbf{E}(t) = \frac{E_0}{\sqrt{1+\varepsilon^2}}(\sin\omega t\,\hat{\mathbf{e}}_x - \varepsilon\cos\omega t\,\hat{\mathbf{e}}_y). \tag{25}$$

In this case, the results depend on the angle φ_p and one should integrate over this angle, i.e., it cannot be replaced

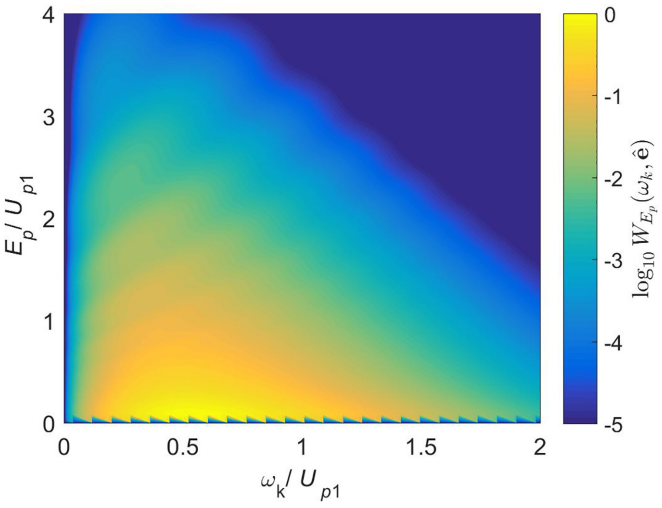

FIG. 8. Logarithm of the rate $W_{E_p}(\omega_k, \hat{\mathbf{e}})$, Eq. (24), presented in the emitted photon energy ω_k-photoelectron kinetic energy E_p plane (in units of the ponderomotive energy U_{p_1}) for ATI of argon atoms by a linearly polarized bichromatic laser field with equal components intensities $I_1 = I_2 = 1.5 \times 10^{14}$ W/cm^2, the fundamental wavelength 1030 nm, and the relative phase $\phi = \pi/2$. The rate is normalized to unity and the false-color scale covers five orders of magnitude.

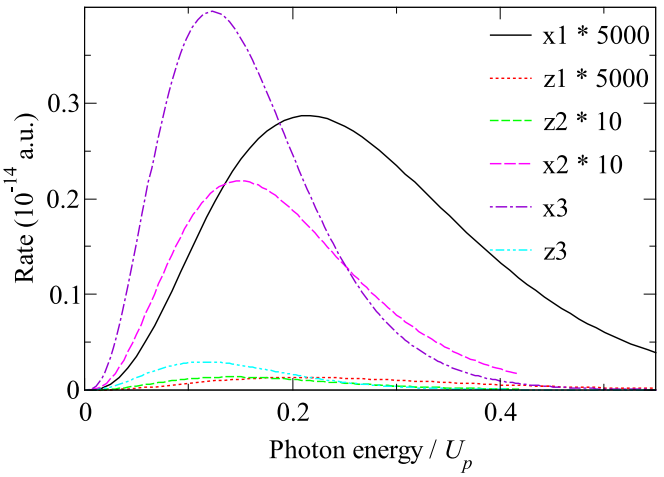

FIG. 9. The total rate $W(\omega_k, \hat{\mathbf{e}}_\mathbf{k})$, Eq. (19), as a function of the emitted photon energy in units of the ponderomotive energy U_p for photon emission during ATI of argon atoms by a circularly polarized laser field, Eq. (25), with $\varepsilon = 1$, the wavelength 1030 nm, and with the intensities $I = j \times 10^{14}$ W/cm^2, $j = 1, 2, 3$, as denoted in the legend by xj for $\hat{\mathbf{e}}_\mathbf{k} = \hat{\mathbf{e}}_x$ and zj for $\hat{\mathbf{e}}_\mathbf{k} = \hat{\mathbf{e}}_z$. The results are multiplied with the factor shown in the legend.

by the factor 2π as in Eq. (21). In addition, the rate depends on the emitted photon polarization direction $\hat{\mathbf{e}}_\mathbf{k}$ (in previous examples we supposed that $\hat{\mathbf{e}}_\mathbf{k}$ is in the polarization direction of the linearly polarized laser electric-field vector). In Fig. 9 we show the results for $\varepsilon = 1$ (circular polarization). Photons are emitted in the direction $\hat{\mathbf{e}}_\mathbf{k} = \hat{\mathbf{e}}_x$ or in the direction $\hat{\mathbf{e}}_\mathbf{k} = \hat{\mathbf{e}}_z$. The results are presented for three different intensities $I = E_0^2 = j \times 10^{14}$ W/cm^2, $j = 1, 2, 3$. The rates for the x component are the same as for the y component and are orders of magnitude higher than the rates for the z component which is perpendicular to the polarization plane. Also, the rates are higher for higher laser intensities and the maximum of the rate as a function of the ponderomotive energy shifts to the lower values with the increase of the intensity (from 0.21 to 0.15 and $0.12U_p$ for $j = 1$, 2, and 3, respectively). The rates for circular polarization are lower than the rate for linear polarization which are shown in Figs. 3–7. In addition, we have checked the results of Fig. 7 using the program which contains the integration over the angle φ_p and which calculates the rate for arbitrary polarizations $\hat{\mathbf{e}}_\mathbf{k}$. We obtained the same results as in Fig. 7 for $\hat{\mathbf{e}}_\mathbf{k}$ in the laser field polarization direction $\hat{\mathbf{e}}_x = \hat{\mathbf{e}}$, while for the directions $\hat{\mathbf{e}}_y$ and $\hat{\mathbf{e}}_z$ we got much lower photon emission rate (for bichromatic field with $\phi = 0$ the maximum rate for these directions is lower by the factor 16 than the rate for the direction $\hat{\mathbf{e}}_\mathbf{k} = \hat{\mathbf{e}}_x$). Finally, we present numerical results for the so-called BEOTC field [32], $\mathbf{E}(t) = \mathbf{E}_1(t) + \mathbf{E}_2(t)$, which consists of two coplanar elliptically polarized components in the xy plane. In Fig. 10 we show the results for bicircular field with counterrotating (sign "−" in the second component) and corotating (sign "+") components,

$$\mathbf{E}_1(t) = \frac{E_1}{\sqrt{2}}[\hat{\mathbf{e}}_x \sin(\omega t) - \hat{\mathbf{e}}_y \cos(\omega t)],$$
$$\mathbf{E}_2(t) = \frac{E_2}{\sqrt{2}}[\hat{\mathbf{e}}_y \sin(2\omega t) \mp \hat{\mathbf{e}}_x \cos(2\omega t)]. \tag{26}$$

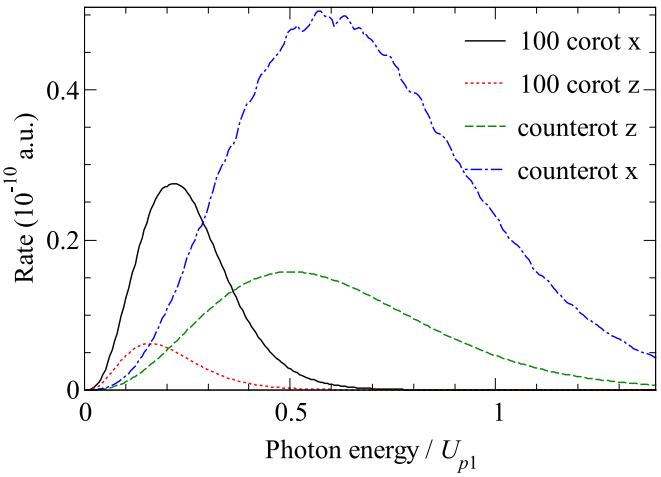

FIG. 10. The total rate $W(\omega_k, \hat{\mathbf{e}}_\mathbf{k})$, as a function of the emitted photon energy in units of the ponderomotive energy U_{p1} for photon emission during ATI of argon atoms by a bicircular field, Eq. (26), with the wavelength 1030 nm and the components intensities $I_1 = I_2 = 1.5 \times 10^{14}$ W/cm^2. For the corotating components the rate is multiplied by the factor 100 and denoted as "100 corot." In the legend we denote by x the rate for $\hat{\mathbf{e}}_\mathbf{k} = \hat{\mathbf{e}}_x$ and by z the rate for $\hat{\mathbf{e}}_\mathbf{k} = \hat{\mathbf{e}}_z$.

We see that the total rate for the counterrotating bicircular field is more than two orders of magnitude higher than that for the corotating field components. The x component of the emitted photon field is equal to the y component and it is much larger than the z component. Comparing the units on the ordinate in Fig. 10 with those of Figs. 3 and 9, we see that the rate for the counterrotating bicircular field is much higher than the rates for linearly and circularly polarized fields.

Orthogonal two-color (OTC) field with the components

$$\mathbf{E}_1(t) = E_1\hat{\mathbf{e}}_x \sin(\omega t), \quad \mathbf{E}_2(t) = E_2\hat{\mathbf{e}}_y \sin(2\omega t + \phi), \quad (27)$$

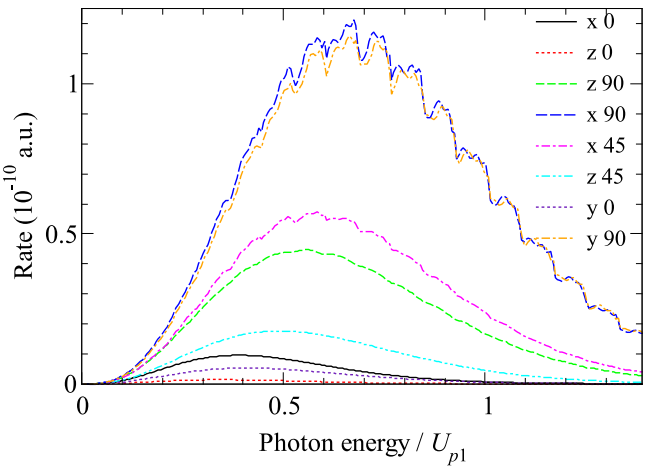

FIG. 11. The total rate $W(\omega_k, \hat{\mathbf{e}}_\mathbf{k})$, as a function of the emitted photon energy in units of the ponderomotive energy U_{p1} for photon emission during ATI of argon atoms by the OTC field, Eq. (27), with the wavelength 1030 nm, the component intensities $I_1 = I_2 = 1.5 \times 10^{14}$ W/cm^2, and the relative phase in degrees as denoted in the legend. The rate for $\hat{\mathbf{e}}_\mathbf{k} = \hat{\mathbf{e}}_x, \hat{\mathbf{e}}_y, \hat{\mathbf{e}}_z$ is denoted by x, y, z, respectively.

is another special case of the BEOTC field. Here $\hat{\mathbf{e}}_x$ and $\hat{\mathbf{e}}_y$ are real unit vectors, which span the xy plane, and ϕ is the relative phase between the two components. In Fig. 11 we show our results for the OTC field with various relative phases. We see that the total rate is the highest for the phase $\phi = \pi/2$ and for the x and y components. For the production of the high-energy photons this case is the most favorable, since it is the highest from all presented field examples and since the maximum appears near $0.7U_{p1}$.

IV. CONCLUSIONS AND DISCUSSIONS

In strong-laser-field-induced processes in experiments observed are the photoelectrons (in ATI) and photons (in HHG). We considered the possibility that, in a single-step process, both photons and electrons are emitted. Using the S-matrix formalism and the SFA we formulated a theory of photon emission during ATI. Our main result is the expression for the rate of simultaneous emission of an electron with the momentum $\mathbf{p}$ and a photon with the energy ω_k and polarization $\hat{\mathbf{e}}_\mathbf{k}$, Eq. (17). The (coincidence) experiments which register simultaneously emission of a photon and of an electron can be challenging. Therefore, we calculated the total photoemission rate integrated over the all electron momenta, Eq. (19). We first considered the case of a linearly polarized laser field, for which calculations are simplified, and found that the corresponding single-atom (microscopic) photon emission rate is many orders of magnitude higher than the HHG rate. For a monochromatic laser field, with a typical wavelength of 1030 nm and the intensity close to the saturation intensity of the Ar atom, the position of the maximum of the total photoemission rate as a function of the photon energy is near $0.2U_p$ (U_p is the ponderomotive energy), i.e., near 5.5 eV, which is lower than the energy of high harmonics. For higher laser intensities and for a bichromatic linearly polarized laser field this peak is shifted to higher energies.

In Figs. 4–6 we have shown that with increasing the laser wavelength and intensity the emitted photon energy shifts to lower values, expressed in units of U_p. Possible explanation of this effect is the change of the regime of ATI, from multiphoton (for shorter wavelength and lower intensity) to tunneling regime. It is possible that the electrons resulting from multiphoton ionization and tunneling ionization do not share energy with the emitted photon in the same way: Tunneling electrons are reluctant to share their energy, while electrons produced in multiphoton ionization share part of their energy with the emitted photon. A similar effect has been observed in the case of dissociative ionization of the H_2^+ molecular ion. Joint energy spectra of the electron E_p and nuclear E_N energies were analyzed in [33,34]. These spectra satisfy the energy-conservation condition $E_N = n\omega - I_p - E_p$, which is analogous to our condition (18). It should be mentioned that simultaneous spectra of ions and electrons can be measured using reaction microscope technique [35].

We have also investigated how the photon emission rate changes if the laser field develops in a plane. In this case numerical calculations are more involved since the integration over the polar angle φ_p should be performed (for a linearly polarized laser field it gives only the factor 2π), and the emitted photon polarization can be arbitrary. We found that

for a monochromatic circularly polarized laser field the total emission rate is lower than in the linearly polarized field case. The total rate for the emitted-photon-polarization x and y directions are the same, while for $\hat{\mathbf{e}}_{\mathbf{k}} = \hat{\mathbf{e}}_z$ the rate is much lower. We have also shown that the rate for the bicircular laser field with the counterrotating components is much higher than the rate for the monochromatic field and the rate for the bicircular field with the corotating components. Finally, we found that the rate for the OTC field is maximum from all the considered cases, in particular for the relative phase $\phi = \pi/2$, which makes this field the most favorable for observation of our photon emission.

Most experimental investigations of HHG are devoted to the analysis of the high-energy spectrum which consists of discrete peaks of high harmonics with photon energy equal to integer multiple of the fundamental photon energy ω. In the early HHG experiments, low-energy continuous radiation was observed as a broad background but has not been investigated (Ref. [36] states the following: "This light emission is incoherent and probably isotropic. Whether there is an underlying continuous background is an open question: these processes should be studied with better resolution and at another detection angle."). In Ref. [37] plasma fluorescence in Ar and Xe gases, called a "2D plasma column," was observed (using a filter which is transparent in 300–700 nm spectral region) and its relationship with the harmonic output signal was investigated. Therefore, it is possible that our photon emission was observed as a background radiation, but its characteristics were not investigated in detail. Furthermore, there is an indication that for the OTC field this background radiation is stronger [38].

On the microscopic level our photon emission is much stronger than the HHG radiation. In order to see what we can expect on the macroscopic level, let us consider a macroscopic system of N_a atoms. The contribution of different atoms add coherently if the phase-matching condition is fulfilled and the probability of HHG increases as N_a^2. However, for our process, due to orthogonality of the ground and continuum atomic states, the number of emitted photons $\langle\psi_{\text{final}}|a_{\mathbf{k}}^{\dagger}a_{\mathbf{k}}|\psi_{\text{final}}\rangle$ [39], leads to an incoherent sum of atomic contributions and the probability increases as N_a. Therefore, if the phase-matching condition is fulfilled, then the HHG radiation should be stronger and our photon emission may be observed as a continuous background at low energies.

HHG photons are emitted in a three-step process, while the photons we consider are emitted during ATI, i.e., in only one step. For HHG it is necessary that the temporarily liberated electron returns to the parent ion so that a HHG photon can be emitted during the recombination. For ultrastrong laser fields the $\mathbf{v} \times \mathbf{B}$ drift of the Lorentz force prevents the return of the electron and the probability of the HHG process decreases quickly with the increase of the laser intensity. We considered this relativistic regime of HHG in Refs. [40,41]. See, for example, Fig. 2 in Ref. [41], where HHG by Ar^{8+} ions ($I_p = 422$ eV), exposed to a Ti:Sa laser ($\lambda = 800$ nm) having the intensity 1.5×10^{18} W/cm^2, was considered. In this example the relativistic HHG rate exhibits a fast decrease (by 100 orders of magnitude in comparison with the nonrelativistic one) with the increase of the harmonic order. However, in our case the optimal emitted photon energy is not affected by this propagation step. The intensities of the order 10^{19} W/cm^2 were achieved in the early 2000s [42] and nowadays ultrahigh intensity ($>10^{22}$ W/cm^2) is in reach [4,5] and requires new spectroscopy techniques in the MeV regime [6]. In addition, since $U_{p1} \propto I\lambda^2$, for longer wavelengths the ponderomotive energy can be much higher (for example, the laser with the wavelength $\lambda = 3.9$ μm was used in Ref. [43]).

Incoherent thermal emission in all directions appears due to scattering process of electron on plasma ions. This continuum-continuum transition is bremsstrahlung emission of laser-produced plasma. The question is how one can distinguish this continuum radiation from the incoherent continuum radiation in our one-step-process photon emission (during ATI). We expect that for lower density of atoms or produced ions the intensity of our radiation is higher than that of the bremsstrahlung radiation. For comparison of these two incoherent emissions a detailed numerical investigation of dependence on macroscopic condition should be done.

In conclusion, we introduced a quantum theory of photon emission during strong-laser-field-induced ionization and presented numerical results for continuous spectrum of the emitted radiation. Since this is the one-step process its probability is orders of magnitude higher than that of the three-step HHG process. Furthermore, in our case much stronger laser fields with longer wavelengths can be used for ionization. The emitted radiation is continuous and incoherent, and a more detailed experimental investigation of this radiation should be done.

ACKNOWLEDGMENTS

We acknowledge support by the Ministry of Science, Higher Education and Youth, Canton Sarajevo, Bosnia and Herzegovina, and useful discussions with Wilhelm Becker and Rui Silva.

[1] G. A. Mourou, T. Tajima, and S. V. Bulanov, Optics in the relativistic regime, Rev. Mod. Phys. **78**, 309 (2006).

[2] F. Krausz and M. Ivanov, Attosecond physics, Rev. Mod. Phys. **81**, 163 (2009).

[3] K. Ueda *et al.*, Roadmap on photonic, electronic and atomic collision physics: I. Light–matter interaction, J. Phys. B **52**, 171001 (2019).

[4] Extreme Light Infrastructure, http://www.eli-laser.eu.

[5] S. Weber *et al.*, P3: An installation for high-energy density plasma physics and ultra-high intensity laser–matter interaction at ELI-Beamlines, Matter Radiat. Extremes **2**, 149 (2017).

[6] S. Y. Luo, P. D. Grugan, Z. Demircioglu, A. Hoos, Z. Germain, R. A. McIntyre, X. Shen, Y. Ji, and B. C. Walker, MeV photoelectron spectrometer for ultraintense laser interactions with atoms and molecules, Rev. Sci. Instrum. **90**, 073104 (2019).

[7] A. McPherson, G. Gibson, H. Jara, U. Johann, T. S. Luk, I. A. McIntyre, K. Boyer, and C. K. Rhodes, Studies of multiphoton production of vacuum-ultraviolet radiation in the rare gases, J. Opt. Soc. Am. B **4**, 595 (1987).

[8] M. Ferray, A. L'Huillier, X. F. Li, L. A. Lompre, G. Mainfray, and C. Manus, Multiple-harmonic conversion of 1064-nm radiation in rare gases, J. Phys. B **21**, L31 (1988).

[9] W. Becker, F. Grasbon, R. Kopold, D. B. Milošević, G. G. Paulus, and H. Walther, Above-threshold ionization: From classical features to quantum effects, Adv. At. Mol. Opt. Phys. **48**, 35 (2002).

[10] M. Lewenstein, M. F. Ciappina, E. Pisanty, J. Rivera-Dean, P. Stammer, Th. Lamprou, and P. Tzallas, Generation of optical Schrödinger cat states in intense laser–matter interactions, Nat. Phys. **17**, 1104 (2021).

[11] J. Rivera-Dean, P. Stammer, A. S. Maxwell, Th. Lamprou, P. Tzallas, M. Lewenstein, and M. F. Ciappina, Light-matter entanglement after above-threshold ionization processes in atoms, Phys. Rev. A **106**, 063705 (2022).

[12] P. Stammer, J. Rivera-Dean, A. Maxwell, Th. Lamprou, A. Ordóñez, M. F. Ciappina, P. Tzallas, and M. Lewenstein, Quantum electrodynamics of intense laser-matter interactions: A tool for quantum state engineering, PRX Quantum **4**, 010201 (2023).

[13] U. Bhattacharya, Th. Lamprou, A. S. Maxwell, A. Ordóñez, E. Pisanty, J. Rivera-Dean, P. Stammer, M. F. Ciappina, M. Lewenstein, and P. Tzallas, Strong–laser–field physics, non–classical light states and quantum information science, Rep. Prog. Phys. **86**, 094401 (2023).

[14] M. E. Tzur, M. Birk, A. Gorlach, M. Krüger, I. Kaminer, and O. Cohen, Photon-statistics force in ultrafast electron dynamics, Nat. Photon. **17**, 501 (2023).

[15] Y. Fang, F.-X. Sun, Q. He, and Y. Liu, Strong-Field Ionization of Hydrogen Atoms with Quantum Light, Phys. Rev. Lett. **130**, 253201 (2023).

[16] D. B. Milošević and F. Ehlotzky, X-ray–atom scattering in the presence of a laser field, Phys. Rev. A **58**, 2319 (1998).

[17] W. Becker, A. Lohr, M. Kleber, and M. Lewenstein, A unified theory of high-harmonic generation: Application to polarization properties of the harmonics, Phys. Rev. A **56**, 645 (1997).

[18] D. B. Milošević, A semi-classical model for high-harmonic generation, in *Super-Intense Laser-Atom Physics, NATO Science Series II: Mathematics, Physics and Chemistry, Vol. 12*, edited by B. Piraux and K. Rzazewski (Kluwer Academic Publishers, Dordrecht, 2001), pp. 229–238.

[19] D. B. Milošević and F. Ehlotzky, Scattering and reaction processes in powerful laser fields, Adv. At. Mol. Opt. Phys. **49**, 373 (2003).

[20] J. R. Taylor, *Scattering Theory: The Quantum Theory of Nonrelativistic Collisions* (Dover, Mineola, NY, 2006).

[21] Dž. Belkić, *Principles of Quantum Scattering Theory* (Institute of Physics Publishing, Bristol, 2004).

[22] L. V. Keldysh, Ionization in the field of a strong electromagnetic wave, Zh. Éksp. Teor. Fiz. **47**, 1945 (1964) [Sov. Phys. JETP **20**, 1307 (1965)].

[23] F. H. M. Faisal, Multiple absorption of laser photons by atoms, J. Phys. B **6**, L89 (1973).

[24] H. R. Reiss, Effect of an intense electromagnetic field on a weakly bound system, Phys. Rev. A **22**, 1786 (1980).

[25] D. B. Milošević, Strong-field approximation and quantum orbits, in *Computational Strong-field Quantum Dynamics: Intense Light-Matter Interactions*, edited by D. Bauer (De Gruyter Textbook, Berlin, 2016), Chap. VII, pp. 199–221.

[26] R. Loudon, *The Quantum Theory of Light* (Clarendon, Oxford, 1983).

[27] D. B. Milošević and F. Ehlotzky, Coulomb corrections in above-threshold ionization in a bichromatic laser field, J. Phys. B **31**, 4149 (1998).

[28] D. B. Milošević, G. G. Paulus, D. Bauer, and W. Becker, Above-threshold ionization by few-cycle pulses, J. Phys. B **39**, R203 (2006).

[29] D. B. Milošević and B. Piraux, High-order harmonic generation in a bichromatic elliptically polarized laser field, Phys. Rev. A **54**, 1522 (1996).

[30] C. Figueira de Morisson Faria, D. B. Milošević, and G. G. Paulus, Phase-dependent effects in bichromatic high-order harmonic generation, Phys. Rev. A **61**, 063415 (2000).

[31] S. Augst, D. D. Meyerhofer, D. Strickland, and S. L. Chin, Laser ionization of noble gases by Coulomb-barrier suppression, J. Opt. Soc. Am. B **8**, 858 (1991).

[32] D. B. Milošević and W. Becker, High-order harmonic generation by bi-elliptical orthogonally polarized two-color fields, Phys. Rev. A **102**, 023107 (2020).

[33] R. E. F. Silva, F. Catoire, P. Rivière, H. Bachau, and F. Martín, Correlated Electron and Nuclear Dynamics in Strong Field Photoionization of H_2^+, Phys. Rev. Lett. **110**, 113001 (2013).

[34] L. Yue and L. B. Madsen, Inter- and intracycle interference effects in strong-field dissociative ionization, Phys. Rev. A **93**, 031401(R) (2016).

[35] J. Ullrich, R. Moshammer, A. Dorn, R. Dörner, L. Ph. H. Schmidt, and H. Schmidt-Böcking, Recoil-ion and electron momentum spectroscopy: Reaction-microscopes, Rep. Prog. Phys. **66**, 1463 (2003).

[36] A. L'Huillier, K. J. Schafer, and K. C. Kulander, Theoretical aspects of intense field harmonic generation, J. Phys. B **24**, 3315 (1991).

[37] E. Takahashi, V. Tosa, Y. Nabekawa, and K. Midorikawa, Experimental and theoretical analyses of a correlation between pump-pulse propagation and harmonic yield in a long-interaction medium, Phys. Rev. A **68**, 023808 (2003).

[38] In preliminary HHG experiments with the OTC field at the Max Born Institute in Berlin this radiation was much stronger than in the pure monochromatic linearly polarized laser field case, so that it completely outshines the high harmonics on the camera and a filter was used to block this radiation (private communication by Anke Heilmann).

[39] D. F. Zaretsky, Ph. Korneev, and W. Becker, High-order harmonic generation in clusters irradiated by an infrared laser field of moderate intensity, J. Phys. B **43**, 105402 (2010).

[40] D. B. Milošević, S. X. Hu, and W. Becker, Quantum-mechanical model for ultrahigh-order harmonic generation in the moderately relativistic regime, Phys. Rev. A **63**, 011403(R) (2000).

[41] D. B. Milošević, S. X. Hu, and W. Becker, Relativistic ultrahigh-order harmonic generation, Laser Phys. **12**, 389 (2002).

[42] E. A. Chowdhury, C. P. J. Barty, and B. C. Walker, "Non-relativistic" ionization of the L-shell states in argon by a "relativistic" 10^{19} W/cm^2 laser field, Phys. Rev. A **63**, 042712 (2001).

[43] T. Popmintchev *et al.*, Bright coherent ultrahigh harmonics in the keV x-ray regime from mid-infrared femtosecond lasers, Science **336**, 1287 (2012).